skin fibroblasts, whereas the amphibian neuropeptide bombesin stimulates Swiss 3T3 mitogenesis (*19*). If biologically active, the aFGF decapeptide would represent a related but unique neuropeptide since it would not contain the amidated carboxyl-terminal methionine residue required for biological activity and receptor binding of these neuropeptides.

Note added in proof. After we submitted this report, the complete amino acid sequence of the 146-residue pituitary-derived bFGF was published (*20*). The complete aFGF and bFGF sequences are 55 percent identical in the commonly aligned regions.

References and Notes

1. O. A. Trowell, B. Chir, E. N. Willmer, *J. Exp. Biol.* **16**, 60 (1939); R. S. Hoffman, *Growth* **4**, 361 (1940).
2. K. A. Thomas, M. Rios-Candelore, S. Fitzpatrick, *Proc. Natl. Acad. Sci. U.S.A.* **81**, 357 (1984).
3. P. Bohlen, F. Esch, A. Baird, K. L. Jones, D. Gospodarowicz, *FEBS Lett.* **185**, 177 (1985); P. Bohlen, A. Baird, F. Esch, N. Ling, D. Gospodarowicz, *Proc. Natl. Acad. Sci. U.S.A.* **81**, 5364 (1984).
4. A. B. Schreiber *et al.*, *J. Cell Biol.*, **101**, 1623 (1985).
5. K. A. Thomas *et al.*, *Proc. Natl. Acad. Sci. U.S.A.* **82**, 6409 (1985).
6. K. A. Thomas, M. C. Riley, S. K. Lemmon, N. C. Baglan, R. A. Bradshaw, *J. Biol. Chem.* **255**, 5517 (1980).
7. R. R. Lobb and J. W. Fett, *Biochemistry* **23**, 6295 (1984).
8. M.-D. Duo, S. S. Huang, J. S. Huang, *Fed. Proc. Fed. Am. Soc. Exp. Biol.* **44**, 695 (1985).
9. D. Gospodarowicz, in *Mediators in Cell Growth and Differentiation*, R. J. Ford and A. L. Maizel, Eds. (Raven, New York, 1985), vol. 37, pp. 109–134.
10. Bovine brain-derived bFGF was purified through the homogenizations, salt precipitations, and CM 50 ion exchange chromatography as described previously (*2*). Material eluted from the CM 50 column was dialyzed against 10 m*M* tris-HCl containing 0.6*M* NaCl (*p*H 7.0), loaded on a heparin-Sepharose column equilibrated in the same buffer, washed extensively with buffer containing 0.6 and 1.0*M* NaCl, and eluted with a 1.5*M* NaCl buffer solution. The eluant was loaded on a C_4 HPLC column and eluted as previously described (*2*). The protein was pure as assessed by high-sensitivity silver-stained 15 percent polyacrylamide electrophoretic gels.
11. M. O. Dayhoff, *Atlas of Protein Sequence and Structure* (National Biomedical Research Foundation, Washington, D.C., 1978), vol. 5, suppl. 3, pp. 345–358.
12. P. T. Lomedico *et al.*, *Nature (London)* **312**, 458 (1984); P. E. Auron *et al.*, *Proc. Natl. Acad. Sci. U.S.A.* **81**, 7907 (1984); C. J. March *et al.*, *Nature (London)* **315**, 641 (1985).
13. T. P. Hopp and K. R. Wood, *Proc. Natl. Acad. Sci. U.S.A.* **78**, 3824 (1981); J. Kyte and R. F. Doolittle, *J. Mol. Biol.* **157**, 105 (1982).
14. R. M. Sweet and D. Eisenberg, *J. Mol. Biol.* **171**, 479 (1983).
15. G. D. Rose, A. R. Geselowitz, G. J. Lesser, R. H. Lee, M. H. Zehfus, *Science*, **229**, 834 (1985).
16. P. Cameron, G. Limjuco, J. Rodkey, C. Bennett, J. A. Schmidt, *J. Exp. Med.*, **162**, 790 (1985); J. Schmidt *et al.*, in *The Physiological, Metabolic, and Immunological Actions of IL-1*, M. J. Kluger, J. J. Oppenheim, M. C. Powanda, Eds. (Liss, New York, in press).
17. J. Van Damme *et al.*, *Nature (London)* **314**, 266 (1985).
18. L. L. Iverson, *Annu. Rev. Pharmacol. Toxicol.* **23**, 1 (1983); N. Minamino *et al.*, *Biochem. Biophys. Res. Commun.* **119**, 14 (1984).
19. J. Nilsson, A. M. von Euler, C. J. Dalsgaard, *Nature (London)* **315**, 61 (1985); E. Rozengurt and J. Sinnett-Smith, *Proc. Natl. Acad. Sci. U.S.A.* **80**, 2936 (1983).
20. F. Esch *et al.*, *Proc. Natl. Acad. Sci. U.S.A.* **82**, 6507 (1985).

21. We thank E. Cordes and E. Scolnick for their support of this work.

20 August 1985; accepted 18 October 1985

A Model for Fibrinogen: Domains and Sequence

Abstract. *Electron microscopy of rotary-shadowed fibrinogen demonstrates that the molecules modified for crystallization by limited cleavage with a bacterial protease retain the major features of the native structure. This evidence, together with image processing and x-ray analysis of the crystals and of fibrin, has been used to develop a three-dimensional low resolution model for the molecule. The data indicate that the two large end domains of the molecule would be composed of the carboxyl-terminus of the Bβ chain (proximal) and γ chain (distal), respectively; the carboxyl-terminus of the Aα chain would fold back to form an additional central domain. On this basis, the carboxyl-terminal region of each of the three chains of fibrinogen is folded independently into a globular domain.*

JOHN W. WEISEL
Department of Anatomy, University of Pennsylvania School of Medicine, Philadelphia 19104
CYNTHIA V. STAUFFACHER
Department of Biological Sciences, Purdue University, West Lafayette, Indiana 47907
ESTHER BULLITT
Graduate Biophysics Program, Brandeis University, Waltham, Massachusetts 02254
CAROLYN COHEN
Rosenstiel Basic Medical Sciences Research Center, Brandeis University

The early trinodular Hall-Slayter model for fibrinogen (*1*), based on electron microscope images of shadowed molecules, has provided a valid, simplified picture of the molecule despite a variety of other conflicting proposals (*2*). Detailed information on the morphology and dimensions of fibrinogen has been derived from analysis of crystalline arrays (*3–9*). Native fibrinogen does not crystallize, but crystals have been produced after limited cleavage of the molecule by a bacterial protease. Image processing of electron micrographs of these ordered arrays had led to an improved structure for the molecule, consisting of a linear arrangement of seven domains, termed the heptad model. This scheme also accounts for the band pattern of fibrin in the electron microscope (*7, 9*). The heptad model differs in detail, however, from some recent electron microscope images of individual molecules (*10–13*). We now show that many of

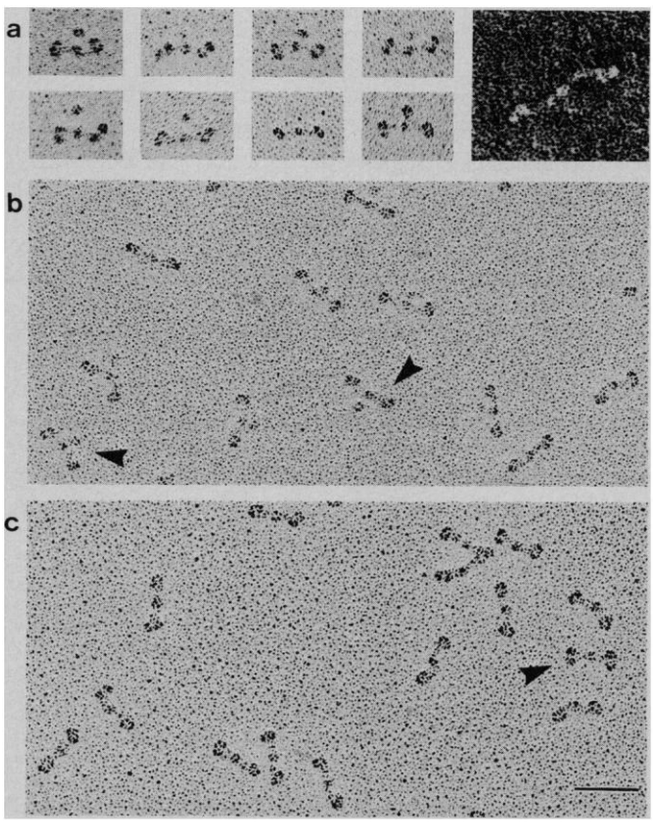

Fig. 1. Electron microscope images of individual, rotary-shadowed bovine fibrinogen molecules. (a and b) Native fibrinogen. (a) A gallery of selected molecules illustrating a range of observed morphologies. The inset (at a higher magnification) shows a negatively stained bovine fibrinogen molecule (*23*) displaying the staggering of the terminal domains. (b) Typical field showing molecules whose overall shape is trinodular. Arrows point to two molecules showing an additional central domain and a subdivision of the end region into two domains. (c) Fibrinogen modified by the *Pseudomonas* protease to a point where crystals are formed (*5*). The molecules are similar to native fibrinogen, but the extra central domain is not seen. The arrow points to a molecule with a distinguishable division of the end domains. The lengths of all molecules average 460 ± 25 Å. Native and modified fibrinogen samples were prepared for electron microscopy and photographed as described in Flicker *et al.* (*24*); scale bar, 500 Å.

these findings can be reconciled by extending the heptad model to three dimensions. We derive this new model, using both image processing of electron micrographs and analysis of low resolution (30 Å) x-ray crystallographic data. These results, together with the findings of others, provide a picture of the molecular morphology of fibrinogen and allow us to correlate the domains with specific regions of the amino acid sequence in the native fibrinogen molecule.

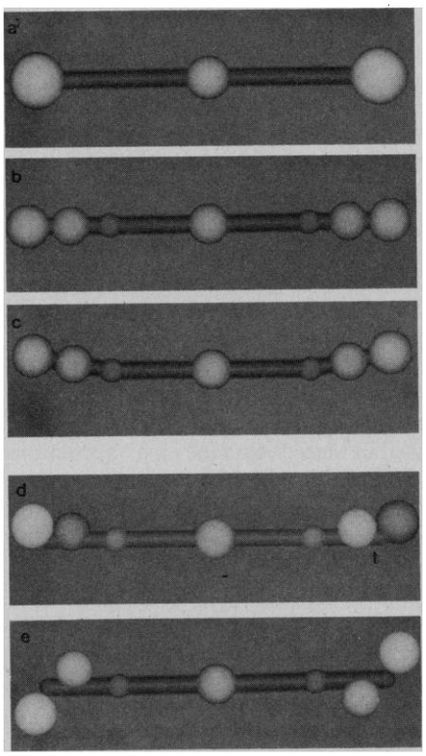

Fig. 2. The evolution of models for the shape of the modified fibrinogen molecule. (a) Trinodular, Hall-Slayter model (*1*). (b) Linear heptad model (*7*). (c) Bent heptad model (*8*). (d) and (e) Two perpendicular views of the three-dimensional model described in this paper. (d) A similar projection to that in (c). (e) View showing lateral displacement of the end domains. The twofold molecular symmetry axis is vertical in the plane of (d) and perpendicular to the page in (e). The proximal and distal ends are shaded differently in (d) to indicate the distance from the observer. The new model in (d) and (e) was deduced by coordinated analysis of electron microscope images (legend to Fig. 3) and 30-Å x-ray data from $P2_1$ crystals (*4–8*). Refinement of fibrinogen models against the x-ray data to 30 Å (105 unique reflections) was carried out by an iterative process with the use of constraints from the image analysis of electron micrographs of the $P2_1$ crystal. Model x-ray intensities were calculated from a simulated crystal structure with trial heptad models expanded to full hydrated volume and packing determined from the analysis of electron microscope images (*6–8*). These data were scaled to the observed x-ray intensities and the model parameters refined to the best fit as judged by the crystallographic *R* factor. Improvements in the *R* factor for models which required the introduction of additional parameters were tested for significance at the 0.005 level by Hamilton's criteria (*25*). The refined model was then used in computer simulations of electron microscope images of the $P2_1$ crystal form. Adjustments to the model, which improved the fit to these images, were made by hand, and the parameters were refined again in the x-ray data. This process was repeated until a satisfactory visual fit of the images was obtained and a stable minimum in the R factor for the x-ray data was reached.

We have examined rotary-shadowed individual fibrinogen molecules by electron microscopy in order to compare the protease-modified molecule to native fibrinogen. Various images are seen in preparations of native bovine fibrinogen (Fig. 1, a and b), and all appear to be closely related to the trinodular Hall-Slayter model. More detailed substructure can also be seen in some of the molecules in these fields. A significant proportion of several thousand molecules examined show some subdivision (often lateral) of the outer domain, but the appearance is variable (*10*). In addition, an extra central domain, first described by Erickson and Fowler (*11*), is displayed by about 25 percent of the molecules.

We have also examined individual molecules of fibrinogen that have been modified by limited proteolysis with a protease from *Pseudomonas aeruginosa* to a point where they form microcrystals and crystals (Fig. 1c). Samples of both digested material before crystallization and redissolved crystals were compared with preparations of the native molecule. In each case, the major difference between the modified and native fibrinogen appears to be the loss of the extra central domain. In the modified molecules, neither the appearance of the major central domain and the outer domains nor the molecular dimensions (460 ± 25 Å) differ substantially from those of native fibrinogen. Subdivision of the outer domain of this modified fibrinogen is also seen at about the same frequency as in the native molecule. These results support our conclusion (*5, 6*) that the modified molecule retains in large part the basic structure of native fibrinogen; they also indicate that the observed mass loss may consist primarily of the small extra central domain.

Electron microscopy and image analysis of negatively stained crystalline arrays are more powerful techniques for determination of macromolecular structure than visualization of individual molecules (*8*). An essential feature of the heptad models derived from such studies of modified fibrinogen is that the two end domains must be located at different distances along the molecular axis from the central domain. In the early heptad models these domains were all colinear, but it was known that the molecule could not be entirely straight since some images could not be fitted without a slight bend at the center of the molecule (*7*). A small bend near the end domains of the molecule (the "bent-heptad" model), rather than at the center, was subsequently found to give a better fit between some of the microcrystal images and the model simulations (*8*) (Fig. 2c). These conclusions were supported by the results of refinements of the heptad models against the x-ray data collected from $P2_1$

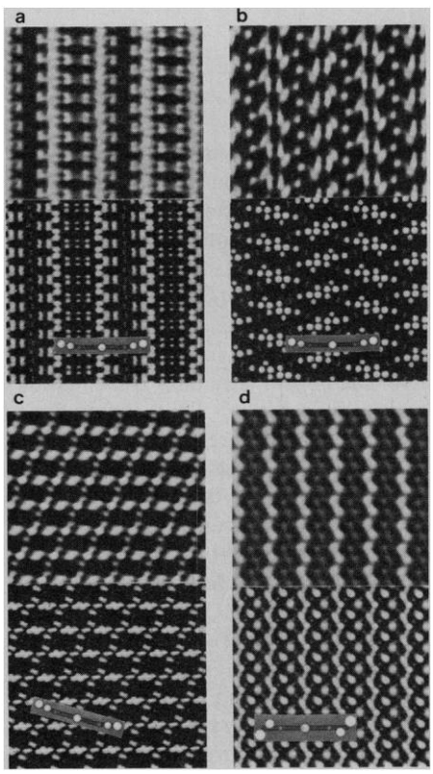

Fig. 3. Computer simulations of electron microscope images of negatively stained crystals and microcrystals of modified fibrinogen. Light areas are regions which are stain-excluding because of the presence of protein, while darker areas allow more stain penetration because of lower protein density. At the top in each case, is a computer-filtered electron microscope image (*7*). At the bottom, is a simulated image of the same crystalline form obtained with the model for fibrinogen shown in Fig. 2, d and e. An inset consisting of one of the molecules in the unit cell (of length 450 Å) is shown for each of the simulations simply to illustrate the molecular orientations. A complicated packing arrangement is required to account for the features in these images (*7*). (a) "Orthogonal sheet" microcrystal form. (b) "Lace" microcrystal form. (c) $P2_1$ crystal form used for x-ray crystallographic studies. This view is along the unique *b* axis. The molecules run in the [−3, 0, 1] direction (*6, 7*). (d) The same crystal form as in (c), but viewed in a near perpendicular direction which corresponds to the major face of these crystals. Techniques for the preparation of modified fibrinogen crystals and microcrystals, their analysis by electron microscopy, and the production of computer simulations of the images have been described (*3–7*).

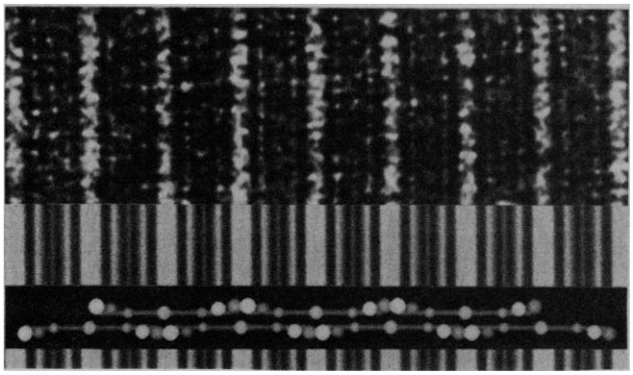

Fig. 4. Computer simulation of the band pattern of negatively stained bovine fibrin. At the top is an electron micrograph of fibrin with an axial repeat of 225 Å. Below is a computer simulation based on the arrangement of molecules shown in the inset. The packing arrangement is complex, but an essential feature is illustrated by a protofibril made up of two half-staggered filaments of molecules bonded end to end (*9*). The three-dimensional version of the model as well as previous heptad models (Fig. 2, b to e) account for this image of fibrin.

crystals of modified fibrinogen (legend to Fig. 2).

By contrast, recent electron micrographs of individual fibrinogen molecules visualized by rotary shadowing often show an apparent lateral division of the outer domain as described above, although some longitudinal separation is also observed (Fig. 1) (*10*). In other studies of individual molecules with negative staining or scanning transmission electron microscopy, this longitudinal displacement is more pronounced (*10–13*) (see Fig. 1a, inset). These apparent dissimilarities may be due in part to differences in preparative techniques including: in rotary shadowing, distortions induced by high surface tension forces; in negative staining, the effects of low *p*H. But all of these images are two-dimensional projections of three-dimensional structures, so that some differences may also correspond to different views of the same structure.

Using computer modeling programs that allow independent placement of the domains in three dimensions, we have now reconciled these findings. The arrangement of the domains was determined by coordinated modeling of both the electron microscope images of crystalline forms and the 30-Å x-ray data without the requirement for linear connectivity. With minimal assumptions, we carried out a search using the 30-Å x-ray data to test a wide range of morphologies. We found a best fit from this class of structures in which the two outer domains are not colinear but are situated off the molecular axis (Fig. 2, d and e). This arrangement gives an overall R factor of 46 percent at 30 Å resolution for the x-ray data [compared with R = 86 percent for a linear heptad model (Fig. 2b) and R = 59 percent for bent heptad models (Fig. 2c)], indicating that the model is beginning to approach the correct structure.

The correspondence between simulations and electron microscope images is also more convincing for this model than for the linear heptad model. The fit is improved for several crystalline arrays, including the orthogonal sheet and lace forms (Fig. 3, a and b), and is most striking for the view of the major face of the $P2_1$ crystal form (Fig. 3d) (*7, 8*). The view of another face of the $P2_1$ crystal is little affected by the changes in the model (Fig. 3c), since the structure is unaltered in this projection (see below). Moreover, the projected structure still accounts for the electron microscope band pattern of fibrin (Fig. 4). As in earlier studies, the presence of the small domain interrupting the rod substantially improves the fit of these images. A compelling aspect of these results is that various different crystal forms, including two views of one crystal, as well as fibrin, can all be well simulated with the same molecular model.

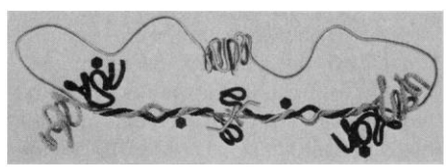

Fig. 5. A schematic representation of the folding of the polypeptide chains in native fibrinogen based on the three-dimensional model for the domains. Various segments of the three pairs of chains in the molecule are assigned to the observed domains. The Aα chain is striped; Bβ is black; γ is light (gray). The disulfide knot is shown at the center with the two coiled-coil regions extending to either side, interrupted by the small plasmin-sensitive domain. The COOH-termini of the Bβ and γ chains fold into globular β and γ domains at the ends, while the COOH-termini of the Aα chains fold back to form an additional central α domain. Disulfide bonds are represented as thin wires holding the chains together at the appropriate locations. Carbohydrate chains bound to the Bβ and γ chains are shown as black hexagons. This view of the model is comparable to that shown in Fig. 2e: the molecular twofold axis is perpendicular to the page, although, for clarity, the COOH-terminal α domain is displaced from the axis. This domain is not seen in the proteolytically modified fibrinogen shown in Fig. 2.

The three-dimensional fibrinogen model can be seen in two perpendicular projections in Fig. 2, d and e. The appearance in one projection is virtually identical to the earlier two-dimensional bent heptad model (Fig. 2c). In the other projection, the domains of the model have a staggered appearance. Both views can be seen in the electron micrographs of rotary-shadowed fibrinogen molecules, whereas negatively contrasted or unstained molecules tend to show the staggered form (see inset, Fig. 1a) (*10–13*). As pointed out by Erickson and Fowler (*11*), the way in which fibrinogen molecules adhere to the different substrates used in these techniques may account in part for these different images. In this new version of the heptad model, the rod portion now extends about 160 Å from the central globular region with an interruption for a small domain and terminates in the two end domains, approximately 50 Å in diameter each, both of which are displaced from the molecular axis. The twofold symmetry axis relating the two halves of the molecule is in the plane of Fig. 2d. This result can be viewed as an extension of earlier models to three dimensions and provides a more accurate picture than previous models of the topology of the end domains. Such a picture fits with recent electron microscope results (*10–12*), particularly those of Williams (*13*).

Previous studies have related parts of the amino acid sequence of fibrinogen to the domains of the Hall-Slayter model, including the central NH_2-terminal "disulfide knot" (*2, 14*) and the three-stranded α-helical coiled-coil rod region (*15, 16*). A major finding in this study concerns the substructure of the outer region of the fibrinogen molecule. The homologous COOH-terminal regions of the Bβ and γ chains have been pictured (*17*) as folding independently into two similar globular regions (displaced an equal distance from the central domain) which together comprise the end domain in the Hall-Slayter model. In the various heptad models, however, these two end domains are displaced along the molecular axis at different distances from the central domain; in the two-dimensional heptad models (Fig. 2, b and c) this colinear arrangement could imply that each of the outer globular domains is formed from all three chains. One of the results of the modeling studies described above is that the two end domains are

also displaced laterally from the molecular axis. These findings may be accounted for simply when the two shortest chains—Bβ and γ—terminate independently in globular regions (β and γ domains). This assignment, as noted by Williams (*13*), follows from the location of the γ-γ cross-linking sites (*18*) at the end of the fibrinogen molecule and from the binding sites involved in fibrin formation at the COOH-terminal end of the γ chains (*19–21*). It is also consistent with other aspects of the amino acid sequence. Although the COOH-terminal sequences of these two chains are highly homologous, there is an additional internal disulfide linkage in the Bβ chains. This linkage could shift the position of the β domain closer to the center of the molecule relative to that of the γ domain.

Erickson and Fowler's study (*11*) also indicated that the COOH-terminal portion of the two longer Aα chains of native fibrinogen folds back from the end of the rod to form a small globular region (an eighth, or α, domain) located near the central region of the molecule. (Since this eighth domain is the extra central region we observe in images of shadowed native fibrinogen, but not in the protease-modified molecules, this portion of the molecule is not represented in heptad models.) The finding that this feature is seen in only some native molecules could be due to superposition with the central domain in some views, to the susceptibility of the Aα chain to proteolysis, or to some unfolding of the structure during preparation for microscopy. Thus, the COOH-terminal region of each of the three chains of fibrinogen appears to be folded independently into a globular domain.

Our suggestion that the protease-modified molecule differs from the native molecule chiefly in the loss of the COOH-terminal portion of the Aα chains is consistent with the fact that the modified molecule retains many biological functions. Cleavage in these flexible single chain regions by the enzyme from *Pseudomonas* and a variety of other enzymes (*4, 6, 8*) appears at present to be a necessary step in crystallizing fibrinogen.

A schematic representation of the folding of the polypeptide chains in fibrinogen, based on the three-dimensional heptad model, is shown in Fig. 5. Here the globular domains of the model are viewed as in Fig. 2e. The central and end domains are connected by a rodlike region shown as a three-chain α-helical coiled coil, interrupted by a small randomly folded, plasmin-sensitive domain made up of all three chains. The β and γ domains are shown for schematic purposes as random coils, since optical rotation studies indicate that the α-helical content of the molecule [about 30 percent (*22*)] can be accounted for by the coiled-coil region. In addition to the seven globular domains in the model, Fig. 5 also depicts the α domain formed by the COOH-termini of the Aα chains folding back to interact at the center of the molecule as would be seen in native fibrinogen.

References and Notes

1. C. E. Hall and H. S. Slayter, *J. Biophys. Biochem. Cytol.* **5**, 11 (1959).
2. Reviews on many aspects of fibrinogen are found in M. W. Mosesson and R. F. Doolittle, Eds., *Molecular Biology of Fibrinogen and Fibrin* (Annals of the New York Academy of Sciences, New York, 1983), vol. 408.
3. N. M. Tooney and C. Cohen, *Nature (London)* **237**, 23 (1972).
4. C. Cohen and N. M. Tooney, *ibid.* **251**, 659 (1974).
5. N. M. Tooney and C. Cohen, *J. Mol. Biol.* **110**, 363 (1977).
6. J. W. Weisel, S. C. Warren, C. Cohen, *ibid.* **126**, 159 (1978).
7. J. W. Weisel, G. N. Phillips, Jr., C. Cohen, *Nature (London)* **289**, 263 (1981).
8. C. Cohen *et al.*, in (*2*), pp. 194–213.
9. J. W. Weisel, G. N. Phillips, Jr., C. Cohen, *ibid.*, pp. 367–379.
10. H. S. Slayter, *ibid.*, pp. 131–145.
11. H. P. Erickson and W. E. Fowler, *ibid.*, pp. 146–163.
12. J. Wall, J. Hainfeld, R. H. Haschemeyer, M. W. Mosesson, *ibid.*, pp. 164–179.
13. R. C. Williams, *ibid.*, pp. 180–193.
14. B. Blombäck, M. Blomback, A. Henschen, B. Hessel, S. Iwanaga, K. R. Woods, *Nature (London)* **218**, 130 (1968).
15. R. F. Doolittle, D. M. Goldbaum, L. R. Doolittle, *J. Mol. Biol.* **120**, 311 (1978).
16. D. L. D. Parry, *ibid.*, p. 545.
17. R. F. Doolittle, *Sci. Amer.* **245**, 126 (December 1981).
18. W. E. Fowler, H. P. Erickson, R. R. Hantgan, J. McDonagh, J. Hermans, *Science* **211**, 287 (1981).
19. B. Blombäck, B. Hessel, D. Hogg, L. Therkildsen, *Nature (London)* **275**, 501 (1978).
20. S. A. Olexa and A. Z. Budzynski, *Proc. Natl. Acad. Sci. U.S.A.* **77**, 1374 (1980).
21. A. Z. Budzynski, S. A. Olexa, B. V. Pandya, in (*2*), pp. 301–304.
22. C. Cohen and A. G. Szent-Györgyi, *J. Amer. Chem. Soc.* **79**, 248 (1957).
23. Kindly provided by R. C. Williams, University of California, Berkeley.
24. P. F. Flicker, T. Wallimann, P. Vibert, *J. Mol. Biol.* **169**, 723 (1983).
25. W. C. Hamilton, *Acta Cryst.* **18**, 502 (1965).

26. We thank B. Elliott and R. C. Williams for comments on the manuscript, S. Almeda for biochemical assistance, J. Black for photography, D. Hellerstein for computing, and L. Seidel for typing. Supported by an Established Investigatorship of the American Heart Association, an NIH grant (HL30954), and a Grant-in-Aid from the Pennsylvania Chapter of the American Heart Association (to J.W.W.); a postdoctoral fellowship from the Arthritis Foundation (to C.V.S.); a Biochemistry Training Grant from NIH (GM07596-07) (to E.B.); a grant from NIH (AM17346) (to C.C.); an NIH-shared instrumentation grant (3-RO1-GM21189-09S1) at Brandeis University to D. J. DeRosier; NIH instrumentation grants at the University of Pennsylvania to John Murray (RR01907), to Terrence Frey (GM28750), and Michael Summers (RR01747), and an NSF grant to Dr. Frank Pepe (PCM82-19960).

14 June 1985; accepted 5 October 1985

Repression of the Immunoglobulin Heavy Chain Enhancer by the Adenovirus-2 E1A Products

Abstract. *The products of the adenovirus-2 (Ad2) immortalizing oncogene E1A repress the activity of the SV40, polyoma virus and E1A enhancers. Evidence is presented that Ad2 infection of MPC11 plasmocytoma cells results in an inhibition of transcription of both the γ2b heavy chain (IgH) and the kappa light chain immunoglobulin genes. This inhibition is caused by the Ad2 E1A products. Furthermore, the Ad2 E1A products repress transcription activated by the immunoglobulin heavy chain enhancer in chimeric recombinants, which are either stably integrated in the genome of lymphoid cells or are present as episomes. The implications of negative regulation of cellular enhancers are discussed.*

René Hen
Emiliana Borrelli
P. Chambon*
Laboratoire de Génétique Moléculaire des Eucaryotes du CNRS, Institut de Chimie Biologique-Faculté de Médecine, 67085 Strasbourg-Cédex (France)

*To whom correspondence should be sent. Telephone: 88371255 (France).

During adenovirus infection E1A is the first gene expressed. Early in infection it yields two messenger RNA's (mRNA's) (12*S* and 13*S*) coding for proteins of 243 and 289 amino acids, respectively. These proteins stimulate transcription of the other early adenovirus genes (*1, 2*) and of a number of cellular genes (*3*). They can also repress the activity of the SV40 and polyoma virus enhancers (*4, 5*). Enhancers are *cis*-acting promoter elements that are required for efficient transcription of some viral and cellular genes and can also activate transcription from heterologous promoters. The activity of some enhancers is restricted to particular cell types or physiological stages and therefore they may have a role in the regulation of gene expression in eukaryotes (*6*). In that expression of the E1A proteins can lead to immortalization of primary cultured cells (*7*), this oncogenic property may possibly be mediated in part by the repression of some cellular enhancers. We have therefore studied the effect of the E1A products on the activity of a well-characterized cellular enhancer, the immunoglobulin heavy